

Neutral Ligands as Potential ^{64}Cu Chelators for Positron Emission Tomography Imaging Applications in Alzheimer's Disease

Yiran Huang, Truc T. Huynh, Liang Sun, Chi-Herng Hu, Yung-Ching Wang, Buck E. Rogers,* and Liviu M. Mirica*



Cite This: *Inorg. Chem.* 2022, 61, 4778–4787



Read Online

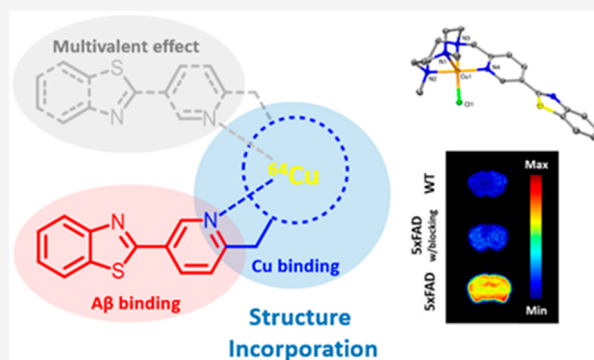
ACCESS |

Metrics & More

Article Recommendations

Supporting Information

ABSTRACT: Positron emission tomography (PET), which uses positron-emitting radionuclides to visualize and measure processes in the human body, is a useful noninvasive diagnostic tool for Alzheimer's disease (AD). The development of longer-lived radiolabeled compounds is essential for further expansion of the use of PET imaging in healthcare, and diagnostic agents employing longer-lived radionuclides such as ^{64}Cu ($t_{1/2} = 12.7$ h, $\beta^+ = 17\%$, $\beta^- = 39\%$, electron capture EC = 43%, and $E_{\text{max}} = 0.656$ MeV) can accomplish this task. One limitation of ^{64}Cu PET agents for neuroimaging applications is their limited lipophilicity due to the presence of several anionic groups needed to ensure strong Cu chelation. Herein, we evaluate a series of neutral chelators containing the 1,4,7-triazacyclononane or 2,11-diaza[3.3]-(2,6)pyridinophane macrocycles that have pyridyl-containing arms incorporating $A\beta$ -peptide-interacting fragments. The crystal structures of the corresponding Cu complexes confirm that the pyridyl N atoms are involved in binding to Cu. Radiolabeling and autoradiography studies show that the compounds efficiently chelate ^{64}Cu , and the resulting complexes exhibit specific binding to the amyloid plaques in the AD mouse brain sections versus wild-type controls.



INTRODUCTION

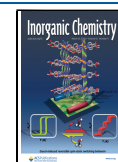
Alzheimer's disease (AD) is the most common neurodegenerative disease. For example, in the United States more than 5 million Americans are living with AD, and this number is expected to reach 16 million by 2050.¹ Positron emission tomography (PET) is a functional imaging technique that can be used for the diagnosis of AD.^{2,3} To date, ^{11}C - and ^{18}F -radiolabeled imaging agents have been tested for PET studies in AD patients, such as Pittsburgh compound B, Florbetapir, and Florbetaben.^{2,4–10} However, the use of these agents is limited because of their short physical half-lives ($t_{1/2} = 20.4$ and 109.8 min for ^{11}C and ^{18}F , respectively) and complicated syntheses.

Therefore, the development of radioimaging agents containing longer-lived radionuclides is important because it would lead to the successful application of diagnostic imaging agents that exhibit improved imaging contrast at longer time points. ^{64}Cu ($t_{1/2} = 12.7$ h) has become a useful radionuclide in the development of radiopharmaceuticals for imaging purposes.^{11–17} The half-life of ^{64}Cu is excellent because it is long enough to allow for imaging at late time points but not so long that it takes weeks to completely decay. In addition, such a half-life will also allow for the imaging agents to be shipped and used in remote areas. Moreover, radiolabeling with ^{64}Cu is always the last step in the synthesis of ^{64}Cu PET imaging agents, thus simplifying their development.¹⁸

One key limitation of ^{64}Cu PET imaging agents is that they could release ^{64}Cu ions in the human body, especially if some ligands have moderate Cu affinity. Also, some enzymes can reduce the chelated Cu^{2+} into Cu^+ , which leads to the further release of ^{64}Cu ions. Consequently, decreasing the free ^{64}Cu level requires ligands to have significantly high metal-binding affinity, limited ligand-exchange kinetics, and also relatively low $\text{Cu}^{\text{II/I}}$ reduction potentials. In our previous report, a series of ^{64}Cu PET imaging multifunctional chelators (MFCs) were obtained by linking the macrocyclic chelators 1,4,7-triazacyclononane (TACN) and 2,11-diaza[3.3]-(2,6)pyridinophane (N4) with $A\beta$ -interacting fragments.^{19–24} The developed MFCs could specifically label the amyloid species and strongly chelate ^{64}Cu and thus could act as potential PET imaging agents for AD. To further increase the metal-binding affinity, larger multidentate ligands were taken into consideration, such as 1,4,7,10-tetraazacyclododecane (cyclen) and 1,4,8,11-tetraazacyclotetradecane (cyclam).^{25–33} In a complementary approach, we decided to investigate chelators based on smaller

Received: February 23, 2022

Published: March 4, 2022



azamacrocycles or azamacrocycles also containing pyridyl groups.^{22,24}

Because previous studies have shown that the metal-binding affinity can be dramatically increased with attachment of the pyridine group to the TACN ligand, herein we introduce a series of ligands designed by employing the strategy of incorporating an $A\beta$ -binding fragment derived from Thioflavin T into the metal-chelating groups TACN and N4 (Figure 1).

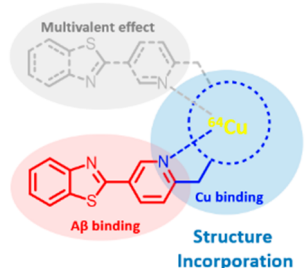


Figure 1. Structure incorporation strategy, with the red oval representing the $A\beta$ -binding fragment and the blue circle representing the metal chelation moiety.

The resulting $A\beta$ -binding framework includes a pyridine ring that can bind to the metal ions to improve the metal-binding affinity of the compounds. The crystal structures of the corresponding Cu complexes confirmed that the pyridine N atoms are involved in Cu binding. Radiolabeling and autoradiography studies show that the compounds efficiently chelate ^{64}Cu , and the resulting complexes exhibit specific binding to the amyloid plaques in AD mouse brain sections versus wild-type (WT) controls.

RESULTS AND DISCUSSION

Design and Synthesis of Bifunctional Chelators and Their Cu Complexes. The chelators were designed through the incorporation strategy by merging chemical structures of the $A\beta$ -binding moiety with a metal-chelating ligand.^{34–37} Furthermore, we have also introduced a second $A\beta$ -binding fragment into the chelator structure to likely increase the $A\beta$ -binding affinity and their lipophilicity, as demonstrated recently,³⁸ while potentially also slightly increasing their metal-binding ability. The synthetic route to these chelators starts with oxidative cyclization of 2-aminothiophenol and 6-methylnicotinaldehyde to generate the 2-(2'-methylpyridyl)-benzothiazole intermediate in 82% yield, followed by its *N*-bromosuccinimide (NBS) bromination at the benzylic position and further conjugation with the TACN- and N4-derived ligands (Scheme 1). The latter ligands were synthesized according to reported procedures.^{24,39}

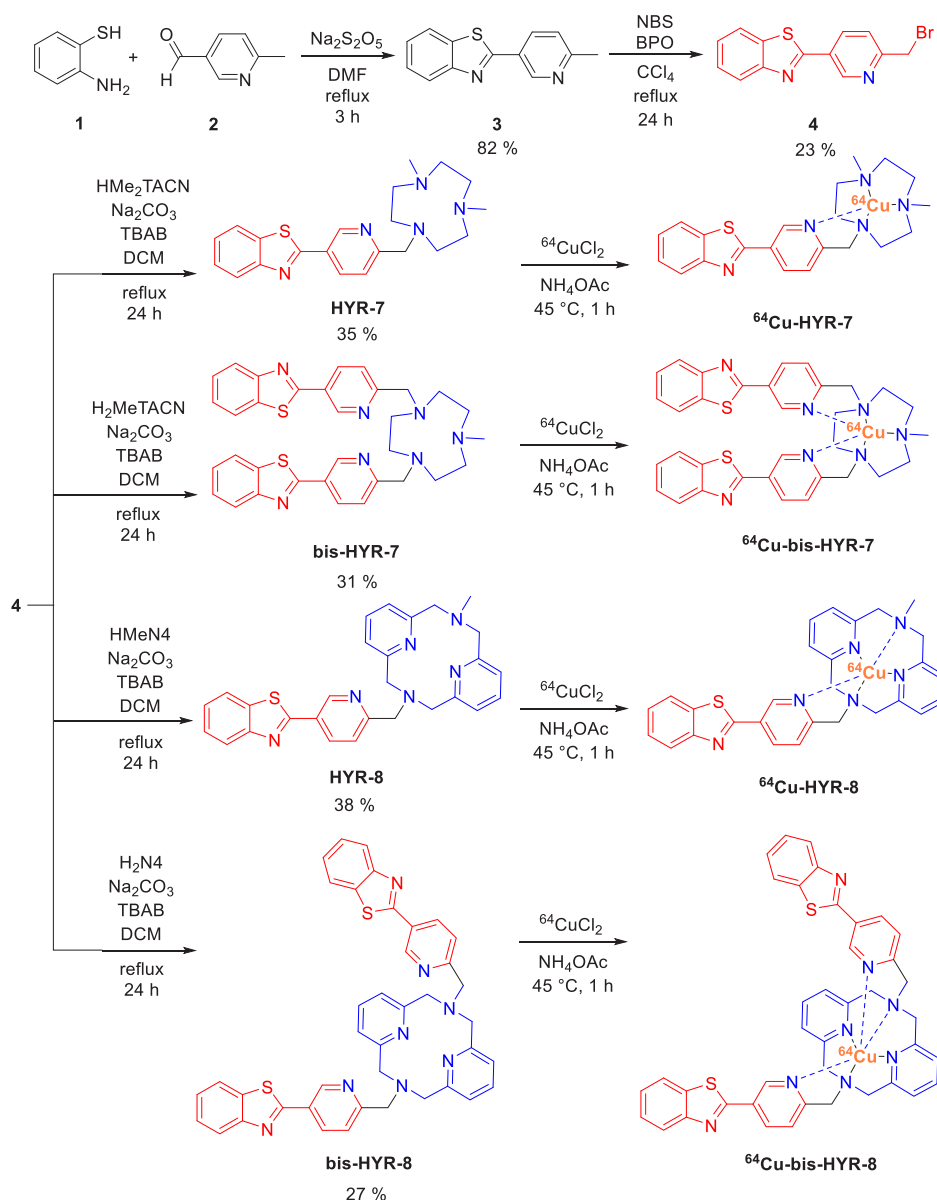
The Cu^{2+} complexes of HYR-7, HYR-8, bis-HYR-7, and bis-HYR-8 were synthesized by mixing equimolar amounts of CuCl_2 with the corresponding ligand in dichloromethane (DCM) or in an aqueous solution. The stability of the resulting Cu complexes was evaluated by monitoring their d–d absorption band by UV–vis, which revealed that these complexes are stable for more than 5 days at room temperature (RT; Figure S5). However, these Cu complexes decompose within minutes in 2.5 M HCl at RT, corresponding to half-lives of <1 min under these conditions and suggesting that these Cu complexes are less kinetically stable than those supported by similar chelators bearing anionic pyridylcarboxylate arms.^{37,40–44} For generation of the ^{64}Cu -radiolabeled com-

plexes, the chelators were reacted with $^{64}\text{CuCl}_2$ in 0.1 M NH_4OAc (pH 5.5). Importantly, complete ^{64}Cu chelation by these ligands was confirmed by radio-high-performance liquid chromatography (HPLC; Figure 2), with no free ^{64}Cu being observed and thus further supporting their use in radiochemistry studies. ^{64}Cu complexes were generated with a radiochemical yield of >95% and used without further purification (see below).

X-ray Structures of Cu Complexes. The Cu-HYR-7 complex was synthesized, and single crystals were obtained by the slow evaporation of a dichloromethane/ether solution. In Cu-HYR-7, the Cu center exhibits a N4Cl square-pyramidal coordination environment, with three N atoms from the TACN macrocycle, one pyridine N atom, and one Cl atom (Figure 3a). The Cu-HYR-8 complex was also obtained by the slow evaporation of an acetonitrile/ether solution under N_2 . In the crystal structure, the Cu center shows a N5 square-pyramidal coordination structure, with four N atoms from the N4 macrocycle and one pyridine N atom (Figure 3b) and similar to Cu complexes supported by related TACN-methylpyridyl or TACN-methylthiazolyl ligands.^{37,40–44} Most importantly, these crystal structures offer solid evidence that the N atom on the pyridine group does interact with the Cu center, and thus the structure incorporation strategy is practical for the design of stronger chelating ligands.

Electron Paramagnetic Resonance (EPR) Spectra of Cu Complexes. To further characterize the Cu-chelator complexes, their X-band EPR spectra were recorded in frozen glasses at 77 K. The EPR spectrum of the Cu-HYR-7 mononuclear complex in a 1:3 (v/v) acetonitrile (MeCN)/propyl cyanide (PrCN) frozen solution reveals a pseudoaxial EPR pattern with three different *g* values: $g_x = 2.059$, $g_y = 2.050$, and $g_z = 2.220$ (Figure 4). Similarly, the EPR spectrum of the Cu-HYR-8 mononuclear complex in 1:3 (v/v) MeCN/PrCN reveals a pseudoaxial EPR pattern with two different *g* values: $g_x = g_y = 2.090$ and $g_z = 2.270$ (Figure S6). For Cu-bis-HYR-7, its EPR spectrum exhibits a pseudoaxial EPR pattern with three different *g* values: $g_x = 2.059$, $g_y = 2.058$, and $g_z = 2.236$ (Figure S7), suggesting that the complex remains mononuclear in solution, while the EPR spectrum of Cu-bis-HYR-8 cannot be simulated, likely because of the presence of two different conformations in solution for this Cu complex (Figure S8). Overall, all of these EPR spectra suggest these Cu complexes adopt a 5-coordinate N/O coordination environment in a likely square-pyramidal geometry.^{24,45,46}

5xFAD Mouse Brain Section Staining of Metal Complexes. Fluorescence imaging studies of 5xFAD mouse brain sections were performed to evaluate the $A\beta$ -binding ability of the developed compounds and Cu complexes. Brain sections from 11-month-old 5xFAD mice were treated with HYR-7, HYR-8, bis-HYR-7, and bis-HYR-8, respectively (Figure S9). Interestingly, results reveal significant fluorescent staining of the amyloid plaques, as confirmed by costaining with the CF594-conjugated HJ3.4 antibody (CF594-HJ3.4), which binds to a wide range of $A\beta$ species.^{2–4,11,47,48} Then, fluorescence staining using the corresponding Cu complexes was also performed because the actual PET imaging agents would be the ^{64}Cu -radiolabeled complexes. All Cu(II) complexes stained well the $A\beta$ plaques, as confirmed by CF594-HJ3.4 antibody immunostaining, suggesting that the Cu(II) complexes could be used for the detection of $A\beta$ species (Figure 5).

Scheme 1. Synthetic Routes and Structures of the Developed Chelators^a

^aThe metal-binding parts and Aβ-interacting fragments are shown in blue and red, respectively.

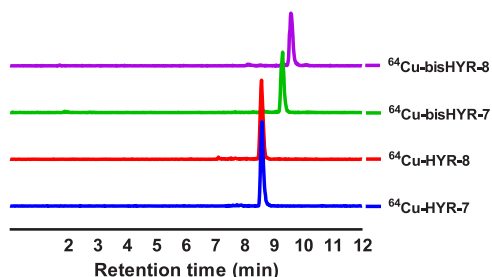


Figure 2. Radio-HPLC chromatographic profiles from ⁶⁴Cu radiolabeling. The retention times were 8:34, 8:34, 9:16, and 9:33 min for ⁶⁴Cu-HYR-7, ⁶⁴Cu-HYR-8, ⁶⁴Cu-bis-HYR-7, and ⁶⁴Cu-bis-HYR-8, respectively. Free ⁶⁴Cu would elute at a retention time of ~2 min.

Autoradiography Studies of ⁶⁴Cu Complexes. *Ex vivo* autoradiography studies using brain sections of transgenic 5x3FAD and age-matched WT mice were also performed to

determine the specific binding to the amyloid plaques for the ⁶⁴Cu-HYR-7, ⁶⁴Cu-HYR-8, ⁶⁴Cu-bis-HYR-7, and ⁶⁴Cu-bis-HYR-8 complexes. There is a great contrast between the intensity of WT (Figure 6a, first row) and 5x3FAD (Figure 6a, third row) for all radiolabeled complexes, especially for ⁶⁴Cu-HYR-7 with a quantified value of 6.3 (Figure 6b). Moreover, the specific binding of the ⁶⁴Cu-labeled complexes to amyloid plaques was confirmed by blocking with the nonradioactive blocking agent B1 (Figure S10), which led to a markedly decreased autoradiography intensity (Figure 6a, second row). In addition, one crucial factor for PET imaging agents of AD is that they need to efficiently cross the blood–brain barrier (BBB). log *D* values between 0.9 and 2.5 have been reported to be optimal for promising BBB permeability.⁴⁹ The ⁶⁴Cu-HYR-7 and ⁶⁴Cu-HYR-8 complexes show relatively low log *D* values because of their dicationic nature. However, with the introduction of a second hydrophobic fragment, the ⁶⁴Cu-bis-HYR-7 and ⁶⁴Cu-bis-HYR-8 complexes exhibit higher log

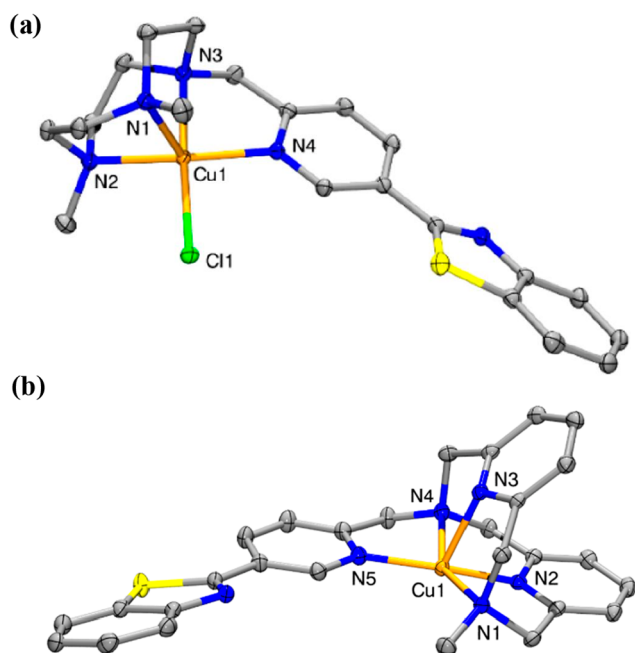


Figure 3. ORTEP plots of the cations: (a) **Cu-HYR-7** at the 50% probability level. Perchlorate anions and H atoms are omitted for clarity. Selected bond lengths (Å): Cu1–N1 2.2189(13), Cu1–N2 2.0871(14), Cu1–N3 2.0396(13), Cu1–N4 2.0313(13), Cu1–Cl1 2.2483(4). (b) **Cu-HYR-8** at the 50% probability level. Selected bond lengths (Å): Cu1–N1 2.2881(18), Cu1–N2 1.9347(18), Cu1–N3 2.1706(18), Cu1–N4 2.1146(19), Cu1–N5 1.9773(18).

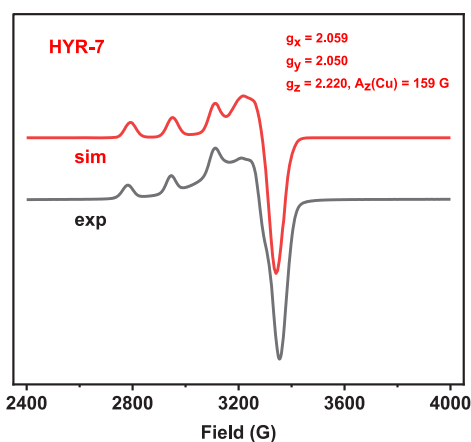


Figure 4. EPR spectra of the **Cu-HYR-7** mononuclear complex in 1 M 1:3 MeCN/PrCN at 77 K. The following parameters were used for the simulations: $g_x = 2.059$, $g_y = 2.050$, $g_z = 2.220$, and $A_z(\text{Cu}) = 159$ G.

D values, suggesting that they have the potential to cross the BBB (Figure 6c). As a result, the latter two complexes were selected to be used in *in vivo* biodistribution studies. Finally, we tested the stability of the radiolabeled complexes $^{64}\text{Cu-bis-HYR-7}$ and $^{64}\text{Cu-bis-HYR-8}$ upon incubation with human serum at 37 °C for up to 24 h (Figure 7). Excitingly, both ^{64}Cu complexes are >85% intact after 20 h of incubation with human serum, further supporting that the Cu complexes should be kinetically stable *in vivo*.

Biodistribution Studies. After promising *in vitro* results were obtained, *in vivo* biodistribution experiments were performed to investigate the pharmacokinetics of ^{64}Cu -

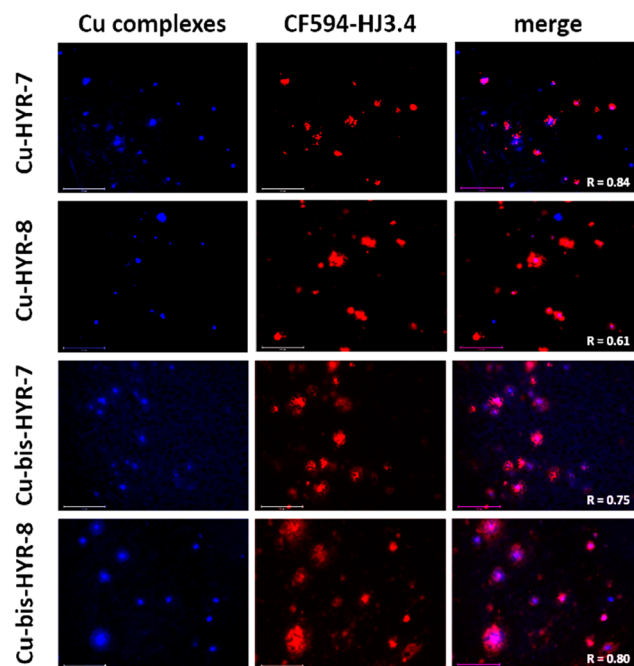


Figure 5. Fluorescence microscopy images of 5xFAD mice brain sections incubated with metal-chelating Cu complexes. The fluorescence signals from compounds and the CF594-HJ3.4 antibody were monitored under blue and red channels, respectively. Scale bar: 125 μm . R is Pearson's correlation coefficient.

radiolabeled complexes using normal CD-1 mice to evaluate the potential of the Cu complexes to cross the BBB; if their BBB permeabilities were high, then further radioimaging studies would be performed in AD mice. The retention and accumulation of the ^{64}Cu -radiolabeled complexes in selected organs were evaluated at 2, 60, and 240 min postinjection (Figure 8). Interestingly, $^{64}\text{Cu-bis-HYR-7}$ showed higher brain uptake at 2 min, with an appreciable accumulation of the radioactivity of $\sim 0.4\%$ ID/g even after 4 h (Figure 8c,e). By comparison, $^{64}\text{Cu-bis-HYR-8}$ exhibited a lower brain uptake of $\sim 0.2\%$ ID/g at 2 min, yet an increased brain accumulation of $\sim 0.4\%$ ID/g was observed after 4 h (Figure 8d,f). These results suggest that $^{64}\text{Cu-bis-HYR-8}$ may take a longer time to reach the brain, possibly given its larger molecular weight and a slower passive diffusion through the BBB. Overall, the brain uptake of these developed ^{64}Cu complexes is slightly lower than those of the complexes we reported previously^{22,38,50,51} or the $^{64}\text{Cu-GTSM}^{52,53}$ or $^{64}\text{Cu-ATSM}^{14}$ derivatives reported by Blower et al. and Donnelly et al., respectively, probably because of the neutral nature of these chelators that cannot balance the positive charge of the Cu^{2+} ion and thus limits the BBB permeability of the Cu complexes. However, the surprising increase over time in brain uptake and somewhat limited rapid liver and kidney clearance observed for $^{64}\text{Cu-bis-HYR-8}$, which is different from what was observed for “free” ^{64}Cu acetate,^{52,53} suggests that the **bis-HYR-8** ligand framework, upon further derivatization, may support Cu complexes that are kinetically stable *in vivo*.⁵⁴

Taken together, these studies provide evidence that the $A\beta$ -binding complexes $^{64}\text{Cu-bis-HYR-7}$ and $^{64}\text{Cu-bis-HYR-8}$ show promise for specific $A\beta$ binding and detection *in vivo*, yet further structure modification is necessary to increase their kinetic stability and BBB permeability for imaging applications. Such structural modifications could include the introduction of

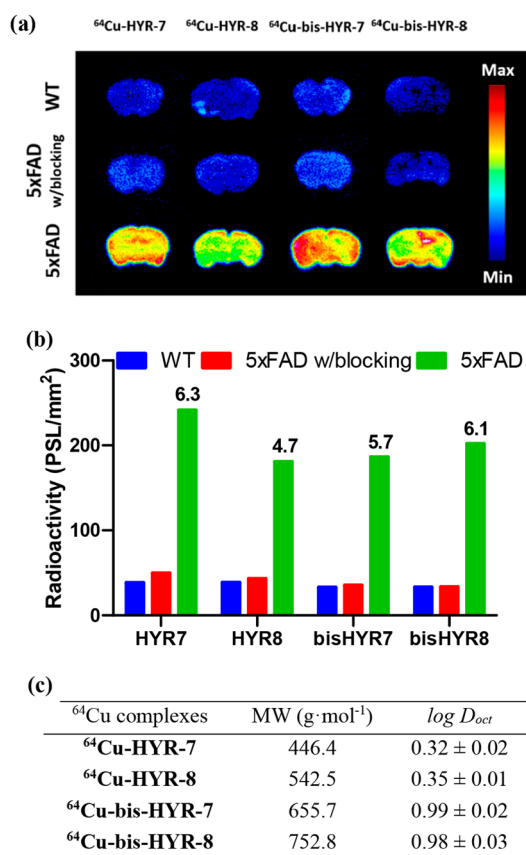


Figure 6. (a) Autoradiography images of the brain sections from WT and 5xFAD mice after the treatment of ^{64}Cu complexes in the absence or presence of a blocking agent. (b) Average intensities of the brain sections in the autoradiography images. The numbers in the bar graph are the intensity ratios of 5xFAD to WT in each group. (c) Partition coefficient ($\log D_{\text{oct}}$) of the corresponding ^{64}Cu complexes in octanol/PBS (pH 7.4).

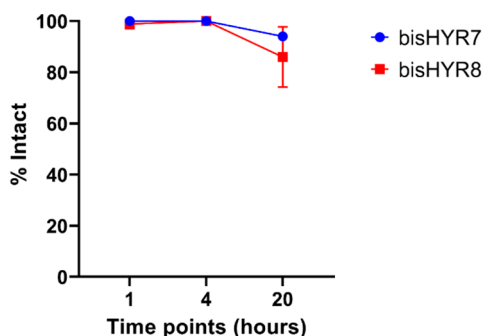


Figure 7. Stability of ^{64}Cu -bis-HYR-7 and ^{64}Cu -bis-HYR-8 upon incubation in the presence of human serum at 37 °C for up to 20 h.

carboxylate or phenolate arms linked to the N atom(s) of the N4 or TACN ligand. The resulting hexadentate ligand should strongly chelate Cu ions to generate 6-coordinate, neutral Cu^{2+} complexes, which are expected to be more hydrophobic and thus exhibit increased BBB permeability.

CONCLUSIONS

In conclusion, a series of TACN- and N4-based chelators with methylpyridylbenzothiazolyl arms were designed and synthesized by incorporating $A\beta$ interacting fragments into the metal-

binding chelating ligands. These ligands are resembling the previously reported TACN-methylpyridyl,^{37,41,42} and TACN-methylthiazolyl ligands,^{43,44} all of which exhibit appreciable Cu-binding properties to be potentially used for ^{64}Cu chelation for PET imaging applications. This incorporation strategy is expected to increase the metal-binding affinity of the $A\beta$ -interacting aryl-benzothiazolyl fragment, without the loss of $A\beta$ specificity. Although the Log D values and BBB permeability of the investigated Cu complexes are less than optimal, this strategy could lead to improved Cu-chelating and $A\beta$ -binding compounds for ^{64}Cu PET imaging in AD. While the introduction of a second $A\beta$ -interacting fragment increases the lipophilicity of the corresponding ^{64}Cu -labeled complexes, it is not likely to significantly increase their Cu-chelating affinity, as shown for the related TACN-methylthiazolyl systems.^{37,40–43} One potential solution could be the introduction of carboxylate or phenolate arms linked to the N atom(s) of the N4 or TACN ligand, an approach similar to the successful development of the related TACN picolinate or TACN methylthiazolylcarboxylate ligands.^{37,40–44} The resulting hexadentate ligand should strongly chelate Cu ions to form 6-coordinate, neutral Cu^{2+} complexes, which are expected to be more hydrophobic and thus exhibit increased BBB permeability.³⁸

Overall, the employed approach based on the incorporation strategy could potentially be applied to other ^{64}Cu -based diagnostic PET imaging applications in neurodegenerative diseases.

EXPERIMENTAL SECTION

General Methods. All reagents were purchased from commercial sources and used as received unless stated otherwise. 1,4-Dimethyl-1,4,7-triazacyclononane (HMe₂TACN), 1-methyl-1,4,7-triazacyclononane (H₂MeTACN), N-methyl-2,11-diaza[3.3](2,6)pyridinophane (HMeN4), and 2,11-diaza[3.3](2,6)pyridinophane (H₂N4) were synthesized according to reported procedures.^{22,24} Solvents were purified prior to use by passing through a column of activated alumina using an MBraun SPS. All solutions and buffers were prepared using metal-free Millipore water that was treated with Chelex overnight and filtered through a 0.22 μm nylon filter. ¹H (500 MHz) NMR spectra were recorded on a Bruker 500 spectrometer (500 MHz). Chemical shifts are reported in parts per million downfield from tetramethylsilane. UV-vis spectra were recorded on a Varian Cary 50 Bio spectrophotometer and are reported as λ_{max} nm (ϵ , M⁻¹ cm⁻¹). All fluorescence measurements were performed using a SpectraMax M2e plate reader (Molecular Devices). A ThermoScientific Orion Star A211 pH meter and ThermoScientific Orion 9110DJWP double junction Micro pH electrode with a Ag/AgCl double junction internal reference (the probe itself was filled with KCl) were used for pH measurements. The pH electrode was calibrated daily with standard solutions of pH 1, 7, and 10. Electrospray ionization mass spectrometry (ESI-MS) experiments were performed by the Mass Spectrometry Lab at UIUC using a Waters Q-TOF Ultima ESI mass spectrometer with an electron spray ionization source. HYR-7, HYR-8, bis-HYR-7, and bis-HYR-8 were dissolved in dimethyl sulfoxide to prepare 10.0 mM stock solutions. The formation of 1:1 Cu/ligand complexes was also confirmed by high-resolution ESI-MS analysis, which revealed the formation of [(L)Cu(formate)]⁺ ions in MS because formic acid was used in the MS sample preparation.

log D Measurements. The compound in octanol (0.5 mL) was subjected to partitioning with octanol-saturated phosphate-buffered saline (PBS; 0.5 mL). The resulting mixture was stirred vigorously for 5 min and centrifuged at 2000 rpm for 5 min. The octanol layer was separated from the PBS layer, and its fluorescence spectrum was recorded (excited at 305 nm). The above PBS layer was partitioned with PBS-saturated octanol (0.5 mL); the octanol layer was separated

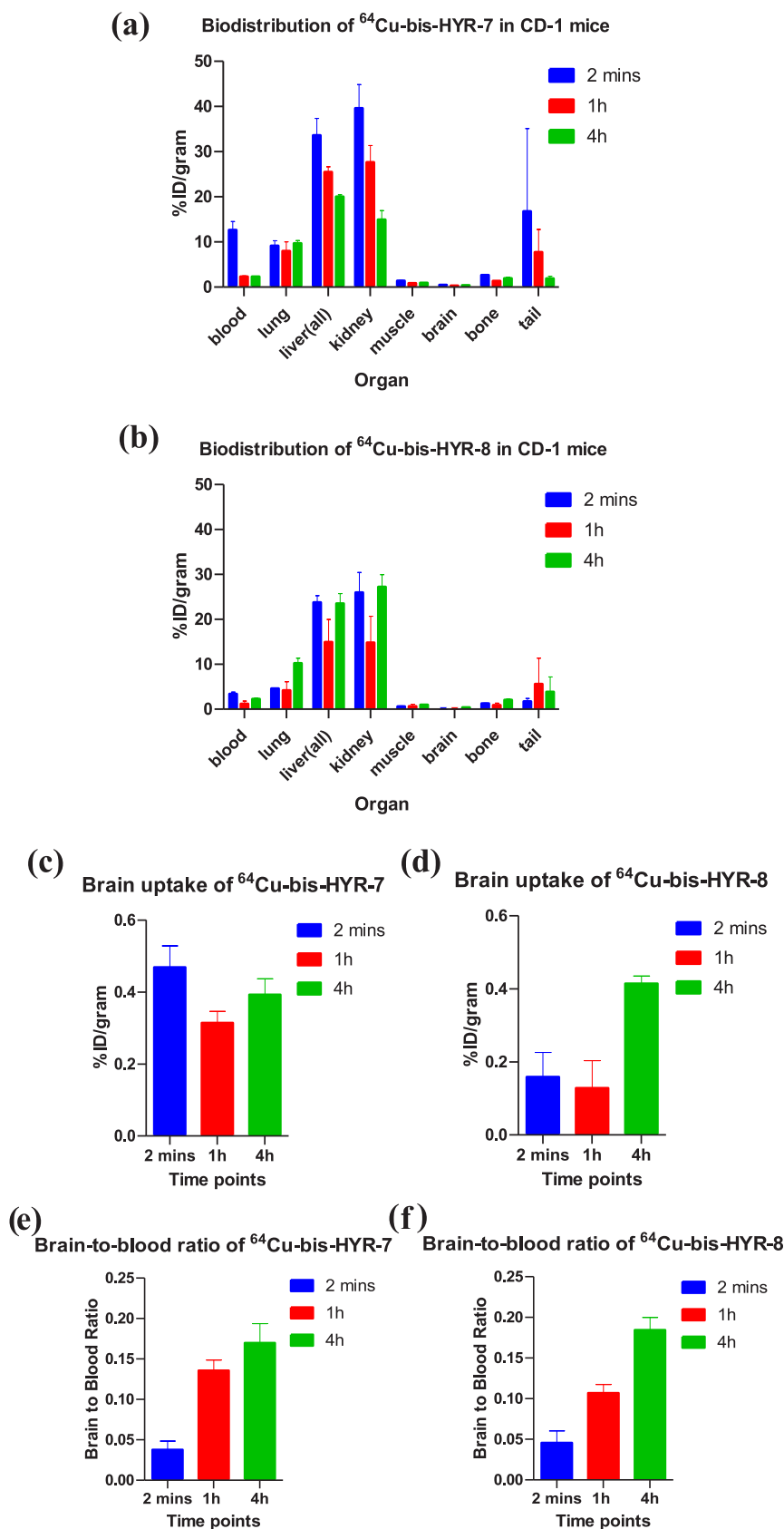


Figure 8. Biodistribution studies of (a) ^{64}Cu -bis-HYR-7 and (b) ^{64}Cu -bis-HYR-8 in the organs of CD-1 mice at 2, 60, and 240 min postinjection (% injected dose per gram, % ID/g). Brain uptake for (c) ^{64}Cu -bis-HYR-7 and (d) ^{64}Cu -bis-HYR-8. Calculated brain-to-blood ratios from biodistribution studies for (e) ^{64}Cu -bis-HYR-7 and (f) ^{64}Cu -bis-HYR-8. The analyzed data were expressed as mean \pm standard deviation ($n = 3$).

after 5 min of vigorous stirring and 5 min of centrifugation at 2000 rpm, and its spectrum was recorded. The log D value was calculated by the fluorescence intensity ratio at 400 nm for the above two octanol extractions. Concentration: 40 μM in a mixture of octanol (0.5 mL) and PBS (0.5 mL).

X-ray Crystallography. The intensity data were collected on a Bruker D8 Venture Kappa diffractometer equipped with a Photon II CPAD detector. An $I\mu\text{s}$ microfocus Mo source ($\lambda = 0.71073 \text{ \AA}$) coupled with a multilayer mirror monochromator provided the incident beam. The sample was mounted on a 0.3 mm nylon loop with the minimal amount of Paratone-N oil. Data were collected at 100 K using a cold stream of $\text{N}_2(\text{g})$ provided by an Oxford Cryostream 700 LT device. Preliminary unit cell constants were determined with a set of 24 narrow-frame scans. Data were collected as a series of φ and/or ω scans with a typical scan width of 0.5° and counting times of 10–30 s/frame at a crystal-to-detector distance of $\sim 3.7 \text{ cm}$. The collection, cell refinement, and integration of the intensity data were carried out with APEX3 software.⁵⁵ The final cell constants were determined by the global refinement of reflections from the complete data set. A multiscan absorption correction was performed with SADABS.⁵⁶ The structure was phased with intrinsic methods using SHELXT⁵⁷ and refined with the full-matrix least-squares program SHELXL.⁵⁸

EPR. An EPR tube was charged with a solution of Cu-HYR-7, Cu-HYR-8, Cu-bis-HYR-7, or Cu-bis-HYR-8 in 1:3 MeCN/PrCN, and then it was frozen in liquid nitrogen. Typical experimental conditions: frequency $\approx 9.418698 \text{ GHz}$, power = 0.6325 mW, modulation frequency = 100 kHz, modulation amplitude = 5 G, and time constant = 327 ms. EPR spectral simulation and analysis were performed using the Bruker WINEPR SimFonia program, version 1.25.

Histological Staining of 5xFAD Mice Brain Sections. Eight-month-old 5xFAD transgenic mice brain sections were blocked with bovine serum albumin (2% BSA in PBS, pH 7.4, 10 min) and covered with a PBS solution of compound and Congo Red (5 μM) for 60 min. The sections were treated with BSA again (4 min) to remove any compound nonspecifically bound to the tissue. Finally, the sections were washed with PBS (3 \times 2 min), deionized water (2 min), and mounted with nonfluorescent mounting media. For antibody staining, the brain sections were incubated with a CF594-conjugated anti-A β antibody (CF594-6E10 antibody) solution (1:1000 dilution in a blocking solution) at RT for 1 h instead of Congo Red. The brain sections were then washed with PBS (3 \times 2 min) and mounted with mounting media. The stained brain sections were imaged using a Zeiss LSM 7010 confocal fluorescent microscope.

Radiolabeling. ^{64}Cu was produced by a (p, n) reaction on enriched ^{64}Ni on a TR-19 biomedical cyclotron (Advanced Cyclotron Systems Inc., British Columbia, Canada) at Mallinckrodt Institute of Radiology, Washington University School of Medicine, and purified with an automated system using standard procedures. A 0.5–1 μL aliquot of $^{64}\text{CuCl}_2$ in 0.01 M HCl was added to 10 μL of 0.1 M ammonium acetate (NH_4OAc) of pH 5.5. Labeling of the chelators with ^{64}Cu was achieved by adding 20 μL of 1 mM compounds to 7.4 MBq (200 μCi) of $^{64}\text{CuCl}_2$ in 100 μL of 0.1 M NH_4OAc of pH 5.5. The resultant solution (pH 5.0–5.5) was allowed to react for 20–60 min at 45 $^\circ\text{C}$ with agitation (1000 rpm) on a thermomixer. A 10 μL aliquot of radiolabeled products was assayed by reversed-phase HPLC (Shimadzu 10Avp system). Eluting samples were detected at 250 and 280 nm with a flow rate of 1.0 mL/min. The mobile phase consisted of a buffer system with 0.1% trifluoroacetic acid (TFA)/ H_2O (A) versus 0.1% TFA/MeCN (B) that proceeded from 0% solvent B to 100% solvent B from 0 to 10 min. ^{64}Cu -labeled complexes were obtained in a high radiochemical yield of greater than 95% and therefore used without further purification.

Lipophilicity Studies of ^{64}Cu -Labeled Complexes. A 5 μL aliquot of ^{64}Cu -labeled complexes (0.37 MBq, 10 μCi) was added to a two-phase system consisting of an organic *n*-octanol and aqueous buffer PBS of pH 7.4 (500 μL /each). The mixture was vortexed at 1000 rpm for 1 h to allow distribution of the radiolabeled compound between the two phases and then given 30 min without agitation for the layers to separate. Aliquots (100 μL) were withdrawn from

aqueous and *n*-octanol layers, and the amount of radioactivity was counted in an automated γ counter. The distribution coefficient was quantified using the following equation of $\log D_{\text{oct}} = \log([M]_{\text{oct}}/[M]_{\text{aq}})$. The experiment was conducted in triplicates of triplicates, and the average of the different measurements was recorded as the final $\log D_{\text{oct}}$ value for each compound.

Ex Vivo Autoradiography Studies. Brain sections of 10-month-old 5xFAD transgenic mice and aged-matched WT mice were immersed in a cryoprotectant solution. These sections were sorted and carefully removed using PBS with a 1% Tween-20 solution, followed by three 10 min rinses in an ice-cold PBS buffer. The sections were placed in a 12-well plate (a single brain slice per well), and $\sim 0.37 \text{ MBq}$ (10 μCi) of ^{64}Cu -labeled chelator in a 2 mL total volume of PBS was added to completely cover the brain section and incubated for 1 h at RT in a shielded bunker. For blocking experiments, the 5xFAD brain sections were incubated with 10 times nonradiolabeled compound 2-(4-hydroxyphenyl)benzothiazole for 10 min and then with ^{64}Cu -labeled chelator. Nonspecific binding was measured as the amount of binding remaining on sections incubated in the additional presence of a blocking agent. After incubation, brain sections were washed three times in ice-cold PBS, mounted on microscope glass slides, and then dried using a cool stream of air. Once the tissue sections were dry, they were mounted on a phosphorimaging screen plate (GE Healthcare Life Sciences) and exposed overnight at $-20 \text{ }^\circ\text{C}$. The imaging plates were read using a Typhoon FLA 9500 biomolecular imager (GE Healthcare Life Sciences). Image analysis was accomplished using ImageJ (version 1.48, public domain) software.

Biodistribution Studies. All animals were handled in accordance with the Guidelines for Care and Use of Research Animals established by the Division of Comparative Medicine and the Animal Studies Committee of Washington University School of Medicine. Animal studies were performed using healthy CD-1 female mice (Charles River Laboratories) of age 5–7 weeks weighing $25.8 \pm 2.1 \text{ g}$. The injection dose was prepared by diluting radiotracers into a 90% saline solution. Mice were injected intravenously into the tail vein with approximately 0.22–0.37 MBq (6–10 μCi) in 100 μL of a saline solution per animal of one of the ^{64}Cu -labeled compounds Cu-bis-HYR-7 or Cu-bis-HYR-8. At different time points (2, 60, and 240 min), mice ($n = 3$ for each group) were sacrificed and tissues of interest (blood, lung, liver, kidney, muscle, brain, bone, and tail) were removed and weighed. Their radioactivity levels were measured with a γ counter and corrected for decay. Radioactivity uptake in the brain and normal tissues was expressed as a percentage of the injected radioactive dose per gram of tissue (% ID/g). All samples were calibrated against a known standard. Prism 8 (version 6.03; GraphPad Software, La Jolla, CA) was used for statistical analysis. Quantitative data were expressed as mean \pm standard deviation, analyzed, and compared using one-way analysis of variance and Student's t test. Differences at the 95% confidence level ($p < 0.05$) were considered statistically significant.

■ ASSOCIATED CONTENT

Supporting Information

The Supporting Information is available free of charge at <https://pubs.acs.org/doi/10.1021/acs.inorgchem.2c00621>.

Experimental procedures, synthetic details, spectrophotometric titrations, UV–vis and fluorescence spectra, radio-HPLC chromatograms, and additional autoradiography data (PDF)

Accession Codes

CCDC 2061721 and 2061722 contain the supplementary crystallographic data for this paper. These data can be obtained free of charge via www.ccdc.cam.ac.uk/data_request/cif, or by emailing data_request@ccdc.cam.ac.uk, or by contacting The Cambridge Crystallographic Data Centre, 12 Union Road, Cambridge CB2 1EZ, UK; fax: +44 1223 336033.

AUTHOR INFORMATION

Corresponding Authors

Liviu M. Mirica – Department of Chemistry, University of Illinois at Urbana–Champaign (UIUC), Urbana, Illinois 61801, United States; Hope Center for Neurological Disorders, Washington University School of Medicine, St. Louis, Missouri 63110, United States; orcid.org/0000-0003-0584-9508; Email: mirica@illinois.edu

Buck E. Rogers – Department of Radiation Oncology, Washington University School of Medicine, St. Louis, Missouri 63108, United States; orcid.org/0000-0001-8189-1797; Email: b.rogers@wustl.edu

Authors

Yiran Huang – Department of Chemistry, University of Illinois at Urbana–Champaign (UIUC), Urbana, Illinois 61801, United States

Truc T. Huynh – Department of Radiation Oncology, Washington University School of Medicine, St. Louis, Missouri 63108, United States; Department of Chemistry, Washington University, St. Louis, Missouri 63130, United States

Liang Sun – Department of Chemistry, University of Illinois at Urbana–Champaign (UIUC), Urbana, Illinois 61801, United States; orcid.org/0000-0002-0080-0855

Chi-Herng Hu – Department of Chemistry, University of Illinois at Urbana–Champaign (UIUC), Urbana, Illinois 61801, United States

Yung-Ching Wang – Department of Chemistry, University of Illinois at Urbana–Champaign (UIUC), Urbana, Illinois 61801, United States

Complete contact information is available at:

<https://pubs.acs.org/10.1021/acs.inorgchem.2c00621>

Notes

The authors declare no competing financial interest.

ACKNOWLEDGMENTS

L.M.M. acknowledges research funding from the NIH (Grant R01GM114588). The authors thank the small animal imaging facility at Washington University School of Medicine for excellent technical assistance, Cedric Mpooy for valuable assistance with animal studies, the Isotope Production Group at Washington University for production of ^{64}Cu , Dr. Toby Woods for help with solving the crystal structures, and Karna Terpstra for obtaining the high-resolution ESI-MS data for the Cu complexes.

REFERENCES

- (1) 2020 Alzheimer's disease facts and figures. *Alzheimer's Dementia* **2020**, *16*, 391.
- (2) Ono, M.; Saji, H. Recent Advances in Molecular Imaging Probes for β -Amyloid Plaques. *MedChemComm* **2015**, *6*, 391.
- (3) Vlassenko, A. G.; Benzinger, T. L. S.; Morris, J. C. PET Amyloid-Beta Imaging in Preclinical Alzheimer's Disease. *Biochim. Biophys. Acta, Mol. Basis Dis* **2012**, *1822*, 370.
- (4) Hayne, D. J.; Lim, S.; Donnelly, P. S. Metal Complexes Designed to Bind to Amyloid- β for the Diagnosis and Treatment of Alzheimer's Disease. *Chem. Soc. Rev.* **2014**, *43*, 6701.
- (5) Villemagne, V. L.; Doré, V.; Burnham, S. C.; Masters, C. L.; Rowe, C. C. Imaging tau and amyloid- β proteinopathies in Alzheimer disease and other conditions. *Nat. Rev. Neurol* **2018**, *14*, 225.
- (6) Choi, S. R.; Schneider, J. A.; Bennett, D. A.; Beach, T. G.; Bedell, B. J.; Zehntner, S. P.; Krautkramer, M. J.; Kung, H. F.; Skovronsky, D. M.; Hefti, F.; Clark, C. M. Correlation of Amyloid PET Ligand Florbetapir F 18 Binding With A β Aggregation and Neuritic Plaque Deposition in Postmortem Brain Tissue. *Alz. Dis. Assoc. Dis* **2012**, *26*, 8.
- (7) Wolk, D. A.; Zhang, Z.; Boudhar, S.; Clark, C. M.; Pontecorvo, M. J.; Arnold, S. E. Amyloid imaging in Alzheimer's disease: comparison of florbetapir and Pittsburgh compound-B positron emission tomography. *J. Neurol. Neurosurg. Psych* **2012**, *83*, 923.
- (8) Carswell, C.; Muckle, K.; Waldman, A.; Win, Z.; Malhotra, P.; Perry, R. Florbetapir Imaging in Clinical Practice: A Retrospective Study of 100 Patients. *J. Neurol. Neurosurg. Psych* **2016**, *87*, e1.101.
- (9) Boccardi, M.; Altomare, D.; Ferrari, C.; Festari, C.; Guerra, U. P.; Paghera, B.; Pizzocaro, C.; Lussignoli, G.; Geroldi, C.; Zanetti, O.; Cotelli, M. S.; Turla, M.; Borroni, B.; Rozzini, L.; Mirabile, D.; Defanti, C.; Gennuso, M.; Prella, A.; Gentile, S.; Morandi, A.; Vollaro, S.; Volta, G. D.; Bianchetti, A.; Conti, M. Z.; Cappuccio, M.; Carbone, P.; Bellandi, D.; Abruuzzi, L.; Bettoni, L.; Villani, D.; Raimondi, M. C.; Lanari, A.; Ciccone, A.; Facchi, E.; Di Fazio, I.; Rozzini, R.; Boffelli, S.; Manzoni, L.; Salvi, G. P.; Cavaliere, S.; Belotti, G.; Avanzi, S.; Pasqualetti, P.; Muscio, C.; Padovani, A.; Frisoni, G. B. Assessment of the Incremental Diagnostic Value of Florbetapir F 18 Imaging in Patients With Cognitive Impairment The Incremental Diagnostic Value of Amyloid PET With [F-18]-Florbetapir (INDIA-FBP) Study. *JAMA Neurol* **2016**, *73*, 1417.
- (10) Khan, S. R.; Patel, N. H.; Wallitt, K. L.; Soneji, N. D.; Fakhry-Darian, D.; Carswell, C. J.; Malhotra, P. A.; Perry, R.; Nijran, K. S.; Khan, S.; Svensson, W.; Barwick, T. D.; Win, Z. First Experience of 100 Clinical F-18 Florbetapir (Amyvid) PET/CT Scans in the Investigation of Cognitive Impairment: Imaging Characteristics, Inter-observer Agreement, Confidence of Read and Clinical Outcomes. *Eur. J. Nucl. Med. Mol. Imaging* **2016**, *43*, S624.
- (11) Sedgwick, A. C.; Brewster, J. T.; Harvey, P.; Iovan, D. A.; Smith, G.; He, X.-P.; Tian, H.; Sessler, J. L.; James, T. D. Metal-based Imaging Agents: Progress towards Interrogating Neurodegenerative Disease. *Chem. Soc. Rev.* **2020**, *49*, 2886.
- (12) Hickey, J. L.; Lim, S.; Hayne, D. J.; Paterson, B. M.; White, J. M.; Villemagne, V. L.; Roselt, P.; Binns, D.; Cullinane, C.; Jeffery, C. M.; Price, R. I.; Barnham, K. J.; Donnelly, P. S. Diagnostic Imaging Agents for Alzheimer's Disease: Copper Radiopharmaceuticals that Target A beta Plaques. *J. Am. Chem. Soc.* **2013**, *135*, 16120.
- (13) Hickey, J. L.; Donnelly, P. S. Diagnostic Imaging of Alzheimer's Disease with Copper and Technetium Complexes. *Coord. Chem. Rev.* **2012**, *256*, 2367.
- (14) McInnes, L. E.; Noor, A.; Kysenius, K.; Cullinane, C.; Roselt, P.; McLean, C. A.; Chiu, F. C. K.; Powell, A. K.; Crouch, P. J.; White, J. M.; Donnelly, P. S. Potential Diagnostic Imaging of Alzheimer's Disease with Copper-64 Complexes That Bind to Amyloid-beta Plaques. *Inorg. Chem.* **2019**, *58*, 3382.
- (15) Fodero-Tavoletti, M. T.; Villemagne, V. L.; Paterson, B. M.; White, A. R.; Li, Q. X.; Camakaris, J.; O'Keefe, G. J.; Cappai, R.; Barnham, K. J.; Donnelly, P. S. Bis(thiosemicarbazonato) Cu-64 Complexes for Positron Emission Tomography Imaging of Alzheimer's Disease. *J. Alz. Dis* **2010**, *20*, 49.
- (16) Chang, A. J.; Sohn, R.; Lu, Z. H.; Arbeit, J. M.; Lapi, S. E. Detection of Rapalog-Mediated Therapeutic Response in Renal Cancer Xenografts Using ^{64}Cu -bevacizumab ImmunoPET. *PLoS One* **2013**, *8*, e58949.
- (17) Nie, X.; Laforest, R.; Elvington, A.; Randolph, G. J.; Zheng, J.; Voller, T.; Abendschein, D. R.; Lapi, S. E.; Woodard, P. K. PET/MRI of Hypoxic Atherosclerosis Using ^{64}Cu -ATSM in a Rabbit Model. *J. Nucl. Med.* **2016**, *57*, 2006.
- (18) Chen, K.; Cui, M. Recent Progress in the Development of Metal Complexes as β -Amyloid Imaging Probes in the Brain. *MedChemComm* **2017**, *8*, 1393.
- (19) Sharma, A. K.; Pavlova, S. T.; Kim, J.; Finkelstein, D.; Hawco, N. J.; Rath, N. P.; Kim, J.; Mirica, L. M. Bifunctional Compounds for Controlling Metal-mediated Aggregation of the A β_{42} Peptide. *J. Am. Chem. Soc.* **2012**, *134*, 6625.

- (20) Sharma, A. K.; Pavlova, S. T.; Kim, J.; Kim, J.; Mirica, L. M. The effect of Cu^{2+} and Zn^{2+} on the $\text{A}\beta_{42}$ peptide aggregation and cellular toxicity. *Metalomics* **2013**, *5*, 1529.
- (21) Sharma, A. K.; Kim, J.; Prior, J. T.; Hawco, N. J.; Rath, N. P.; Kim, J.; Mirica, L. M. Small Bifunctional Chelators That Do Not Disaggregate Amyloid β Fibrils Exhibit Reduced Cellular Toxicity. *Inorg. Chem.* **2014**, *53*, 11367.
- (22) Bandara, N.; Sharma, A. K.; Krieger, S.; Schultz, J. W.; Han, B. H.; Rogers, B. E.; Mirica, L. M. Evaluation of ^{64}Cu -based Radiopharmaceuticals That Target $\text{A}\beta$ Peptide Aggregates as Diagnostic Tools for Alzheimer's Disease. *J. Am. Chem. Soc.* **2017**, *139*, 12550.
- (23) Huang, Y. R.; Cho, H. J.; Bandara, N.; Sun, L.; Tran, D.; Rogers, B. E.; Mirica, L. M. Metal-chelating benzothiazole multifunctional compounds for the modulation and Cu -64 PET imaging of A beta aggregation. *Chem. Sci.* **2020**, *11*, 7789.
- (24) Sharma, A. K.; Schultz, J. W.; Prior, J. T.; Rath, N. P.; Mirica, L. M. Coordination Chemistry of Bifunctional Chemical Agents Designed for Applications in Cu -64 PET Imaging for Alzheimer's Disease. *Inorg. Chem.* **2017**, *56*, 13801.
- (25) El Ghachtouli, S.; Cadiou, C.; Dechamps-Olivier, I.; Chuburu, F.; Aplincourt, M.; Roisnel, T. (Cyclen- and cyclam-pyridine)copper complexes: The role of the pyridine moiety in Cu -II and Cu -I stabilisation. *Eur. J. Inorg. Chem.* **2006**, *2006*, 3472.
- (26) Delgado, R.; Felix, V.; Lima, L. M. P.; Price, D. W. Metal complexes of cyclen and cyclam derivatives useful for medical applications: a discussion based on thermodynamic stability constants and structural data. *Dalton Trans* **2007**, 2734.
- (27) Storr, T.; Thompson, K. H.; Orvig, C. Design of targeting ligands in medicinal inorganic chemistry. *Chem. Soc. Rev.* **2006**, *35*, 534.
- (28) Lima, L. M. P.; Esteban-Gómez, D.; Delgado, R.; Platas-Iglesias, C.; Tripier, R. Monopicolinate Cyclen and Cyclam Derivatives for Stable Copper(II) Complexation. *Inorg. Chem.* **2012**, *51*, 6916.
- (29) Derrick, J. S.; Kim, Y.; Tak, H.; Park, K.; Cho, J.; Kim, S. H.; Lim, M. H. Stereochemistry of metal tetramethylcyclam complexes directed by an unexpected anion effect. *Dalton Trans* **2017**, *46*, 13166.
- (30) Conte-Daban, A.; Beyler, M.; Tripier, R.; Hureau, C. Kinetics Are Crucial When Targeting Copper Ions to Fight Alzheimer's Disease: An Illustration with Azamacrocyclic Ligands. *Chem. Eur. J.* **2018**, *24*, 8447.
- (31) Kim, G.; Lelong, E.; Kang, J.; Suh, J.-M.; Le Bris, N.; Bernard, H.; Kim, D.; Tripier, R.; Lim, M. H. Reactivities of cyclam derivatives with metal-amyloid- β . *Inorg. Chem. Front* **2020**, *7*, 4222.
- (32) Lelong, E.; Suh, J.-M.; Kim, G.; Esteban-Gómez, D.; Cordier, M.; Lim, M. H.; Delgado, R.; Royal, G.; Platas-Iglesias, C.; Bernard, H.; Tripier, R. Complexation of C-Functionalized Cyclams with Copper(II) and Zinc(II): Similarities and Changes When Compared to Parent Cyclam Analogues. *Inorg. Chem.* **2021**, *60*, 10857.
- (33) Derrick, J. S.; Lee, J.; Lee, S. J. C.; Kim, Y.; Nam, E.; Tak, H.; Kang, J.; Lee, M.; Kim, S. H.; Park, K.; Cho, J.; Lim, M. H. Mechanistic Insights into Tunable Metal-Mediated Hydrolysis of Amyloid-beta Peptides. *J. Am. Chem. Soc.* **2017**, *139*, 2234.
- (34) Savelieff, M. G.; Nam, G.; Kang, J.; Lee, H. J.; Lee, M.; Lim, M. H. Development of Multifunctional Molecules as Potential Therapeutic Candidates for Alzheimer's Disease, Parkinson's Disease, and Amyotrophic Lateral Sclerosis in the Last Decade. *Chem. Rev.* **2019**, *119*, 1221.
- (35) Zhang, C.; Gomes, L. M. F.; Zhang, T.; Storr, T. A small bifunctional chelator that modulates $\text{A}\beta_{42}$ aggregation. *Can. J. Chem.* **2018**, *96*, 78.
- (36) Dyrager, C.; Vieira, R. P.; Nyström, S.; Nilsson, K. P. R.; Storr, T. Synthesis and evaluation of benzothiazole-triazole and benzothiazole-triazole scaffolds as potential molecular probes for amyloid- β aggregation. *New J. Chem.* **2017**, *41*, 1566.
- (37) Roger, M.; Lima, L. M. P.; Frindel, M.; Platas-Iglesias, C.; Gustin, J.-F.; Delgado, R.; Patinec, V.; Tripier, R. Monopicolinate-dipicolyl derivative of triazacyclononane for stable complexation of Cu^{2+} and $^{64}\text{Cu}^{2+}$. *Inorg. Chem.* **2013**, *52*, 5246.
- (38) Cho, H. J.; Huynh, T. T.; Rogers, B. E.; Mirica, L. M. Design of a multivalent bifunctional chelator for diagnostic $(^{64})\text{Cu}$ PET imaging in Alzheimer's disease. *Prod. Natl. Acad. Sci. U. S. A* **2020**, *117*, 30928.
- (39) Wessel, A. J.; Schultz, J. W.; Tang, F.; Duan, H.; Mirica, L. M. Improved synthesis of symmetrically & asymmetrically N-substituted pyridinophane derivatives. *Org. Biomol. Chem.* **2017**, *15*, 9923.
- (40) Guillou, A.; Lima, L. M. P.; Roger, M.; Esteban-Gomez, D.; Delgado, R.; Platas-Iglesias, C.; Patinec, V.; Tripier, R. 1,4,7-Triazacyclononane-Based Bifunctional Picolinate Ligands for Efficient Copper Complexation. *Eur. J. Inorg. Chem.* **2017**, *2017*, 2435.
- (41) Bazzicalupi, C.; Bencini, A.; Faggi, E.; Garau, A.; Giorgi, C.; Lippolis, V.; Perra, A.; Valtancoli, B. Encapsulation of metal cations and anions within the cavity of bis(1,4,7-triazacyclononane) receptors. *Dalton Trans* **2006**, 1409.
- (42) Marnett, M.; Aragoni, M. C.; Arca, M.; Atzori, M.; Bencini, A.; Bazzicalupi, C.; Blake, A. J.; Caltagirone, C.; Devillanova, F. A.; Garau, A.; Hursthouse, M. B.; Isaia, F.; Lippolis, V.; Valtancoli, B. Synthesis and Coordination Properties of Quinoline Pendant Arm Derivatives of [9]aneN(3) and [9]aneN(2)S as Fluorescent Zinc Sensors. *Inorg. Chem.* **2009**, *48*, 9236.
- (43) Le Fur, M.; Beyler, M.; Le Poul, N.; Lima, L. M. P.; Le Mest, Y.; Delgado, R.; Platas-Iglesias, C.; Patinec, V.; Tripier, R. Improving the stability and inertness of Cu (II) and Cu (I) complexes with methylthiazolyl ligands by tuning the macrocyclic structure. *Dalton Trans* **2016**, *45*, 7406.
- (44) Guillou, A.; Lima, L. M. P.; Esteban-Gómez, D.; Le Poul, N.; Bartholomä, M. D.; Platas-Iglesias, C.; Delgado, R.; Patinec, V.; Tripier, R. Methylthiazolyl Tacn Ligands for Copper Complexation and Their Bifunctional Chelating Agent Derivatives for Bioconjugation and Copper-64 Radiolabeling: An Example with Bombesin. *Inorg. Chem.* **2019**, *58*, 2669.
- (45) Yokoi, H.; Addison, A. W. Spectroscopic and redox properties of pseudotetrahedral copper(II) complexes. Their relation to copper proteins. *Inorg. Chem.* **1977**, *16*, 1341.
- (46) Klement, R.; Stock, F.; Elias, H.; Paulus, H.; Pelikán, P.; Valko, M.; Mazúr, M. Copper(II) complexes with derivatives of salen and tetrahydrosalen: a spectroscopic, electrochemical and structural study. *Polyhedron* **1999**, *18*, 3617.
- (47) Perrin, R. J.; Fagan, A. M.; Holtzman, D. M. Multimodal Techniques for Diagnosis and Prognosis of Alzheimer's Disease. *Nature* **2009**, *461*, 916.
- (48) Nordberg, A. PET Imaging of Amyloid in Alzheimer's Disease. *Lancet Neurol* **2004**, *3*, 519.
- (49) Dischino, D. D.; Welch, M. J.; Kilbourn, M. R.; Raichle, M. E. Relationship between Lipophilicity and Brain Extraction of C-11-Labeled Radiopharmaceuticals. *J. Nucl. Med.* **1983**, *24*, 1030.
- (50) Sun, L.; Cho, H.-J.; Sen, S.; Arango, A. S.; Huynh, T. T.; Huang, Y.; Bandara, N.; Rogers, B. E.; Tajkhorshid, E.; Mirica, L. M. Amphiphilic Distyrylbenzene Derivatives as Potential Therapeutic and Imaging Agents for the Soluble Amyloid- β Oligomers in Alzheimer's Disease. *J. Am. Chem. Soc.* **2021**, *143*, 10462.
- (51) Wang, Y.; Huynh, T. T.; Cho, H.-J.; Wang, Y.-C.; Rogers, B. E.; Mirica, L. M. Amyloid β -Binding Bifunctional Chelators with Favorable Lipophilicity for ^{64}Cu Positron Emission Tomography Imaging in Alzheimer's Disease. *Inorg. Chem.* **2021**, *60*, 12610.
- (52) Torres, J. B.; Andreozzi, E. M.; Dunn, J. T.; Siddique, M.; Szanda, I.; Howlett, D. R.; Sunassee, K.; Blower, P. J. PET Imaging of Copper Trafficking in a Mouse Model of Alzheimer Disease. *J. Nucl. Med.* **2016**, *57*, 109.
- (53) Andreozzi, E. M.; Torres, J. B.; Sunassee, K.; Dunn, J.; Walker-Samuel, S.; Szanda, I.; Blower, P. J. Studies of copper trafficking in a mouse model of Alzheimer's disease by positron emission tomography: comparison of ^{64}Cu acetate and ^{64}Cu GTSM. *Metalomics* **2017**, *9*, 1622.
- (54) Roca-Sabio, A.; Bonnet, C. S.; Mato-Iglesias, M.; Esteban-Gómez, D.; Tóth, É.; Blas, A. d.; Rodríguez-Blas, T.; Platas-Iglesias, C.

Lanthanide Complexes Based on a Diazapyridinophane Platform Containing Picolinate Pendants. *Inorg. Chem.* **2012**, *51*, 10893.

(55) APEXIII; Bruker AXS, Inc.: Madison, WI, 2018.

(56) Krause, L.; Herbst-Irmer, R.; Sheldrick, G. M.; Stalke, D. Comparison of silver and molybdenum microfocus X-ray sources for single-crystal structure determination. *J. Appl. Crystallogr.* **2015**, *48*, 3.

(57) Sheldrick, G. SHELXT - Integrated space-group and crystal-structure determination. *Acta Crystallogr., Sect. A* **2015**, *71*, 3.

(58) Sheldrick, G. A short history of SHELX. *Acta Cryst. A: Found. Cryst.* **2008**, *64*, 112.

Recommended by ACS

Characteristic Evaluation of a ^{11}C -Labeled Leucine Analog, 1- α -[5- ^{11}C]methylleucine, as a Tracer for Brain Tumor Imaging by Positron Emission Tomography

Tsuyoshi Tahara, Hirotaka Onoe, *et al.*

FEBRUARY 20, 2023

MOLECULAR PHARMACEUTICS

READ 

Recent Advances in Bioorthogonal Click Chemistry for Enhanced PET and SPECT Radiochemistry

Xinlin Zhong, Min Yang, *et al.*

FEBRUARY 22, 2023

BIOCONJUGATE CHEMISTRY

READ 

Synthesis and In Vitro and In Vivo Evaluation of ^{18}F -Labeled Positron Emission Tomography Tracers for Imaging A β Plaques

Wei Zheng, Zehui Wu, *et al.*

FEBRUARY 16, 2023

ACS CHEMICAL NEUROSCIENCE

READ 

Functionalization of Radiolabeled Antibodies to Enhance Peripheral Clearance for High Contrast Brain Imaging

Eva Schlein, Dag Sehlin, *et al.*

OCTOBER 06, 2022

MOLECULAR PHARMACEUTICS

READ 

Get More Suggestions >